ISSN 1541-308X, Physics of Wave Phenomena, 2023, Vol. 31, No. 3, pp. 160–170. © Allerton Press, Inc., 2023.

OPTICAL AND MICROWAVE SPECTROSCOPY OF AQUEOUS SOLUTIONS

Optical and Electron Microscopy of Clusters of Nd^{3+}:LaF_3 Nanoparticles Synthesized by the HTMW Method

G. O. Silaev[a, b], V. N. Krasheninnikov[a], A. T. Shaidulin[b,c], O. V. Uvarov[c], E. O. Orlovskaya[c], Yu. V. Orlovskii[c, d], and Yu. G. Vainer[a, b, *]

[a] *Institute of Spectroscopy of the Russian Academy of Sciences, Moscow, Troitsk, 108840 Russia*
[b] *Higher School of Economics, National Research University, Moscow, 101000 Russia*
[c] *Prokhorov General Physics Institute of the Russian Academy of Sciences, Moscow, 119991 Russia*
[d] *Institute of Physics, University of Tartu, Tartu, 50411 Estonia*
**e-mail: vainer@isan.troitsk.ru*

Received December 31, 2022; revised December 31, 2022; accepted January 10, 2023

Abstract—A comparative study of the sizes and spatial structure of single dielectric colloidal nanoparticles of lanthanum fluoride, doped with rare-earth neodymium ions (Nd^{3+}:LaF_3), and their conglomerates in an aqueous solution has been performed. Nanoparticles were synthesized by aqueous co-precipitation method with subsequent hydrothermal microwave (HTMW) treatment. Experiments were performed using three methods: transmission electron microscopy (TEM), nanoparticle tracking analysis (NTA), and dynamic light scattering (DLS). An analysis of the results has shown that a stable colloidal solution of nanoparticles is formed during synthesis. The solution consists of single lanthanum fluoride nanoparticles, having a narrow (10–30 nm) size distribution, and nanoclusters formed on their basis. It is also shown that the spatial structure of nanoclusters cannot be described in terms of the fractal model, which is widely used to describe clusters formed in colloidal solutions of nanoparticles of various nature.

Keywords: aqueous colloidal solutions of Nd^{3+}:LaF_3 nanoparticles, hydrothermal microwave (HTMW) method, colloidal clusters, ultramicroscope, trajectory analysis, dynamic light scattering (DLS)

DOI: 10.3103/S1541308X23030093

1. INTRODUCTION

Luminescent nanoparticles of lanthanum fluoride Nd^{3+}:LaF_3 have a number of unique properties: narrow absorption and emission lines in the first (0.75–0.95 μm) and second (1–1.2 μm) optical transparency windows of biological tissues, high luminescence quantum yield [1], long excited state lifetimes, possibility of temporal and spectral suppression of the autofluorescence of biological tissues, high photo- and physicochemical stability, and low toxicity. In addition, techniques of synthesizing stable aqueous colloidal solutions of lanthanum fluoride nanoparticles and methods of their doping with rare-earth metal ions have been developed [2]. The above-listed advantages make these nanoparticles highly promising as fluorescent nanoprobes in biological studies and medicine [3–6] and explain the extraordinary importance of studying their physical and chemical properties.

Despite the important advantages, the application of the Nd^{3+}:LaF_3 nanoparticles in bioimaging is limited by several significant factors. First, the absorption of the radiation used to excite fluorescence is insufficiently intense, whereas the fluorescence quenching is strong (in particular, because of the presence of OH groups inside these nanoparticles); these features significantly reduce their luminescence efficiency [2]. Another important problem, causing serious difficulties in real applications of colloidal lanthanum fluoride nanoparticles, is the undesirable processes of aggregation of these nanoparticles in solution during their synthesis and storage. Thus, the studies aimed at developing more efficient methods of synthesizing the aforementioned nanoparticles of higher quality, free to a certain extent of the aforementioned drawbacks, are urgent. It is necessary to gain a better insight into the mechanisms of fluorescence quenching in these crystals and the reasons for their aggregation, as well as to develop ways to suppress these undesirable phenomena. In addition, it is important to control the average sizes of synthesized nanoparticles and their spread in size. When carrying out these investigations, very important problems are those related to the characterization of synthesized nanoparticles, in particular, the possibility of real time control of the sizes and spatial structure of synthesized nanoparticles and conglomerates on their basis.

As is well known, transmission electron microscopy (TEM) is the main method for determining the sizes of colloidal nanoparticles. However, despite the high spatial resolution of this method, which makes it possible to visualize nanoparticles studied at the level of individual atoms, its application for visualizing nanoparticles in colloidal aqueous solutions meets several significant difficulties. This is a complex and not always accessible method, which requires a rather long time to prepare a sample for measurements. In addition, in the case of aqueous solutions of nanoparticles, they must be dried before measurements. Drying of clusters may change significantly their shape and thus distort information about their morphology in solutions. As a rule, studies aimed at developing a technique for fabricating nanoparticles with improved parameters require many syntheses. Therefore, the high efficiency and information content of the experimental methods used to characterize the morphology and sizes of synthesized nanoparticles becomes of prime importance in these studies, since TEM is not entirely efficient in this context.

Methods of optical far-field microscopy are free of most of the aforementioned drawbacks; they are characterized by high efficiency and information content, which includes a much simpler procedure of sample preparation, short measurement time, and insignificant influence on a sample studied. However, the sensitivity of the overwhelming majority of these methods is insufficient for detecting single nanoparticles. We have developed a highly sensitive light-sheet laser ultramicroscope, which makes it possible to visualize in real time the single nanoparticles and clusters in aqueous solutions from elastic light scattering signals and determine on this basis the sizes of these objects by analyzing the individual trajectories of their Brownian motion. This method for determining the sizes of single nanoparticles in a solution is known in the literature as the nanoparticle tracking analysis (NTA) [7]. The sensitivity of this ultramicroscope was improved to a level allowing one to reliably detect single lanthanum fluoride nanoparticles in aqueous solutions up to 20 nm in size and even smaller and track individual trajectories of their Brownian motion.

In this paper we report the results of a comparative study of the sizes and spatial structure of single dielectric colloidal lanthanum fluoride nanoparticles doped with rare-earth neodymium ions (Nd^{3+}:LaF_3) and clusters on their basis; the analysis was performed by the TEM and NTA methods. The former method provided information about the individual sizes of nanoparticles and the nanoclusters based on them in solution, while the latter method made it possible to determine the hydrodynamic radius of nanoclusters. In addition, to compare the results and obtain more correct information about the nanocluster morphology, we measured the nanoparticle sizes by the dynamic light scattering (DLS) method [8], which is widely used to measure nanoparticle sizes in solutions and is based on the photon-correlation spectroscopy of light elastically scattered from the particles under study.

NTA was the main tool of real time monitoring of effective nanoparticle sizes during synthesis. In contrast to the DLS method, which yields information, averaged over a large ensemble of nanoparticles and requires a high concentration of particles studied in solution, NTA allows one to perform measurements at much lower concentrations. In this case, the presence of large foreign particles (for example, micrometer-sized dust particles) in the test solution does not affect the measurement results, in contrast to measurements by the DLS method [9]. In addition, direct visualization of nanoparticles in solution makes it possible to estimate their concentration and control the solution purity.

Below, we present TEM data on the distributions of individual sizes of nanoparticles (without taking into account their agglomeration), which we will call primary nanoparticles, and distributions of the effective sizes of nanoclusters formed due to the primary nanoparticle agglomeration. Two quantities characterizing the spatial structure of nanoclusters are used as effective sizes. These are (i) the radius of gyration, which is widely used to determine the effective sizes of clusters of various nature and is determined by numerical analysis of the TEM images of observed nanoclusters, and (ii) the hydrodynamic radius, which is determined experimentally, applying the developed ultramicroscope and the DLS method.

2. EXPERIMENTAL

Nanoparticles of Nd^{3+}:LaF_3 were synthesized by aqueous co-precipitation method with subsequent hydrothermal microwave (HTMW) treatment [1, 2, 10]. They were characterized by a narrow size distribution; the neodymium ion concentration was controlled (up to 50 at %). Primary nanoparticles and clusters formed based on them were studied. When carrying out NTA and DLS measurements, nanoparticles were located in an aqueous solution placed in an optical quartz cell. To monitor the stability of colloidal solutions of nanoparticles, the ζ potential was also measured. When performing NTA, DLS, and ζ-potential measurements, solutions were diluted with purified deionized water to concentrations of $\sim 5 \times 10^{-5}$, $\sim 10^{-1}$, and $\sim 2 \times 10^{-2}$ mg/mL, respectively. Before all measurements, the solutions were treated in an ultrasonic bath for at least 10 min. In the case of TEM analysis, nanoparticles were deposited on a standard carbon nanofilm, installed on a Lavsan substrate, using

the spin-coating procedure [11]. To this end, a drop of solution with a particle concentration of ~10^{-2} mg/mL was deposited on a rapidly rotating (3000 rpm) carbon substrate, leaving single nanoparticles on it. This approach made it possible to observe nanoparticles under conditions excluding their superposition and thus significantly attenuating the undesirable processes of their interaction during solution drying. TEM measurements were performed using a Zeiss Libra 200FE HR electron microscope (Carl Zeiss, Germany) at an accelerating voltage of 200 kV. DLS and ζ-potential measurements of nanoparticles were performed using a Zetasizer Nano ZS instrument (Malvern Instruments Ltd., Worcestershire, UK) with a laser wavelength of 633 nm at a temperature of 25°C.

To implement the NTA method, we used a highly sensitive dark-field light-sheet ultramicroscope developed by us. This instrument makes it possible to visualize the Brownian motion of nanoparticles in different transparent liquids and determine their concentration and size distribution. The main distinctive feature of this ultramicroscope is the elimination of the interfering action of the speckle pattern, arising because of the high degree of spatial coherence of the laser source of light used to illuminate a sample [12]. This is implemented by transmitting the radiation of the laser source (diode laser, λ = 405 nm, 100 mW) through an optical multimode quartz waveguide with a fiber diameter 100 μm, subjected to random mechanical deformation with a frequency of 150 periods/s. Random spatial and temporal modulation of the phase front of the laser beam transmitted through the waveguide is performed in this way, reducing the spurious influence of speckles on recorded nanoparticle images. The waveguide output radiation, used for phase modulation of the laser beam, is converted into an astigmatic beam using cylindrical optics; one of the foci of this beam is directed inside the cuvette to a selected area in the liquid volume, forming an illuminated area (close to planar) oriented perpendicular to the observation axis. This area is referred to as the light sheet. The thickness of this sheet varies from several micrometers to several tens of micrometers. Due to the small thickness of the illuminated region, the liquid and particles beyond it do not contribute to the measured signal. As a result, the microscope acquires a high sensitivity, which, in our case, makes it possible to record reliably the individual trajectories of single nanoparticles up to 20 nm in size. The solution was placed in a transparent quartz optical cell with internal transverse sizes of 10 × 10 mm and height from 10 to 50 mm. The radiation elastically scattered by nanoparticles located in the light-sheet region is recorded by a sensitive CCD camera (PCO Sensicam em, Excelitas PCO GmbH, Germany), operating in the continuous mode with a frame rate of 13.1 Hz. A block diagram of the microscope is shown in Fig. 1. Some examples of images of single nanoparticles obtained in the developed ultramicroscope are shown in Fig. 2.

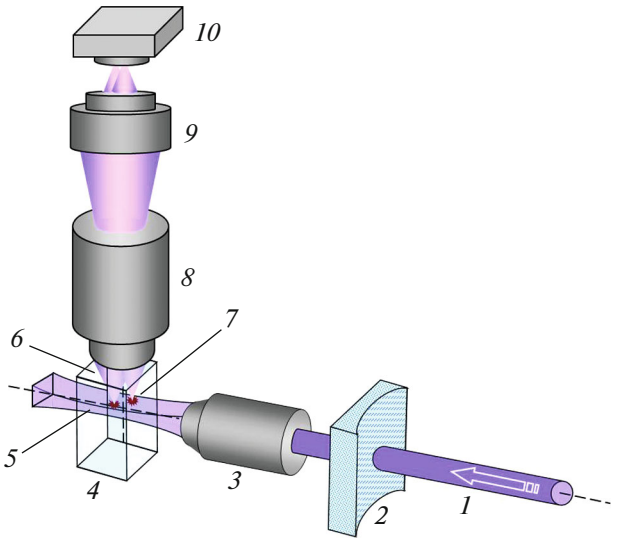

Fig. 1. (Color online) Block diagram of laser dark-field light-sheet ultramicroscope for detecting single nanoparticles in aqueous solutions from elastic light scattering signals: (*1*) laser beam transmitted through a spatial modulator, (*2*) cylindrical lens, (*3*) focusing objective, (*4*) optical cuvette, (*5*) illuminated volume in the form of a light sheet, (*6*) radiation scattered by nanoparticles, (*7*) nanoparticles located in the illuminated volume, (*8*) collecting microlens, (*9*) camera objective, and (*10*) CCD camera.

Analysis of the information obtained with the ultramicroscope is reduced to determination of the coordinates of "centroid" of individual nanoparticle images observed in the lateral plane for each frame and subsequent determination of the trajectories of their Brownian motion. On this basis the root-mean-square displacement values d^2 (the first stage) for each nanoparticle in the lateral projection are calculated. The ImageJ program [13] and built-in TrackMate plugin [14] were used for this purpose. Then, based on the data obtained, the values of the individual hydrodynamic radius, R_h, were determined for each observed nanoparticle using the Stokes–Einstein formula [15, 16]:

$$\overline{d}^2 = \frac{2K_B T t}{3\pi R_h \eta}, \quad (1)$$

where K_B is the Boltzmann constant, T is temperature, t is the total measurement time, and η is the dynamic viscosity of the medium. Measurements were performed at T = 22.5°C, and η was assumed to be 0.943 mPa s.

When analyzing trajectories, it is necessary to take into account the drift of nanoparticles caused by the presence of convective fluid flows in the measuring cell. The direction of the observed drift may be different at different points of the measured volume and change over time. Convection may arise as a result of

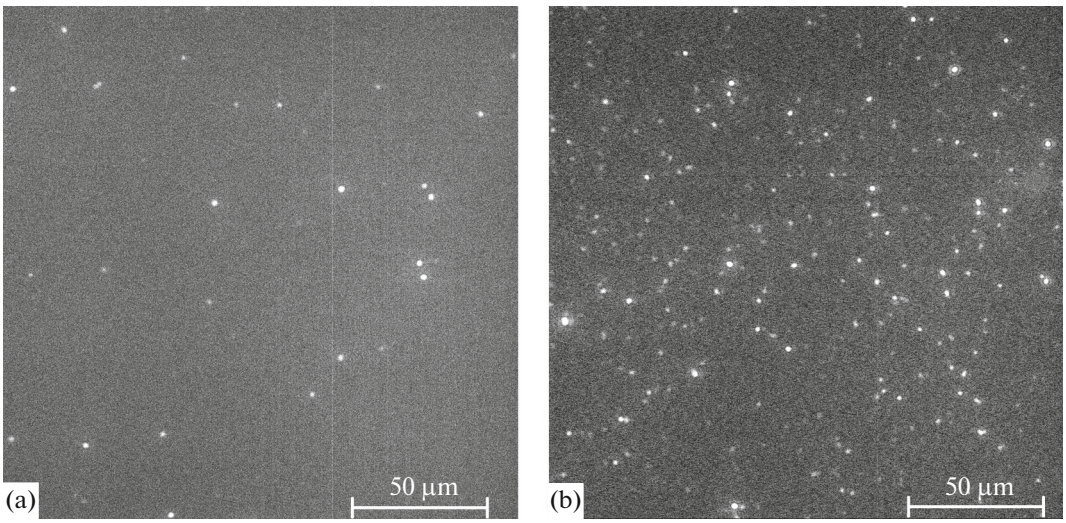

Fig. 2. Images of single colloidal Nd^{3+}:LaF_3 nanoparticles in water, recorded using the developed ultramicroscope at low (a) and higher (b) nanoparticle concentrations.

poor temperature stabilization of the sample, as well as due to the absorption caused by laser beam heating. Figure 3 shows an example of distribution of average nanoparticle velocities in the sample, calculated from the measured trajectories in the presence of convection.

The distribution is noticeably shifted relative to the zero position, which suggests a significant contribution of convection to the trajectories of observed nanoparticles. In our measurements, to reduce convective flows, the solution under study was poured into the measuring cell to a height of no more than 5–6 mm, and passive temperature stabilization conditions were created in the surrounding volume. The influence of the residual contribution of the convection was eliminated computationally using a corresponding shift of coordinates in the velocity space (Fig. 4). These measures made it possible to exclude almost completely the influence of convection on the results of the analysis.

The individual size of synthesized nanoparticles with their aggregation disregarded (i.e., the size of primary nanoparticles) was determined as the radius of a circle of equal area. To characterize the effective size of clusters of complex shape, we applied the characteristic that is often used in this case: radius of gyration, R_g [17]. Since we deal with a two-dimensional image, we first calculated the R_g value for the observed nanocluster in the image plane using the general formula

$$R_g = \sqrt{\frac{1}{2N^2}\sum_{i=1}^{N}\sum_{j=1}^{N}\left(\overline{r}_i - \overline{r}_j\right)^2}, \qquad (2)$$

where N is the number of primary particles in a cluster and r_i are their coordinates. Then the radius of gyration for the corresponding three-dimensional cluster was determined by corresponding recalculation with a factor $k = 1.24$ (according to [18]).

Figure 5 shows an example of relationship between the radius of gyration and the model cluster geometry.

3. RESULTS AND DISCUSSION

Typical TEM images of colloidal Nd^{3+}:LaF_3 nanoparticles synthesized in an aqueous solution on a carbon substrate are shown in Fig. 6. It can be seen in these images that most of observed nanoparticles are aggregated into clusters having a complex spatial structure and sizes up to 200 nm in certain directions. The aggregation of colloidal nanoparticles is a well-known effect. It can be considered as undesirable, hindering the use of these particles in most of applications. Therefore, the study of the mechanism of nanoparticle aggregation and search for ways to suppress it is an important and urgent problem. Note that on the substrate we observe practically flat aggregates, the size and structure of which could change in one way or another as a result of drying.

To analyze the spatial structure of clusters, another parameter is also widely used: the hydrodynamic radius R_h. Both parameters, R_g and R_h, make it possible to characterize the effective sizes of clusters; however, they are based on different physical properties of the latter. The radius of gyration characterizes the spatial distribution of the masses of particles composing a cluster, while the hydrodynamic radius characterizes its hydrodynamic resistance. The latter parameter is determined by both the structure of a cluster and the parameters of its interaction with the environment, primarily, by the viscosity of the surrounding liquid and the hardness of the crystal framework. It is conve-

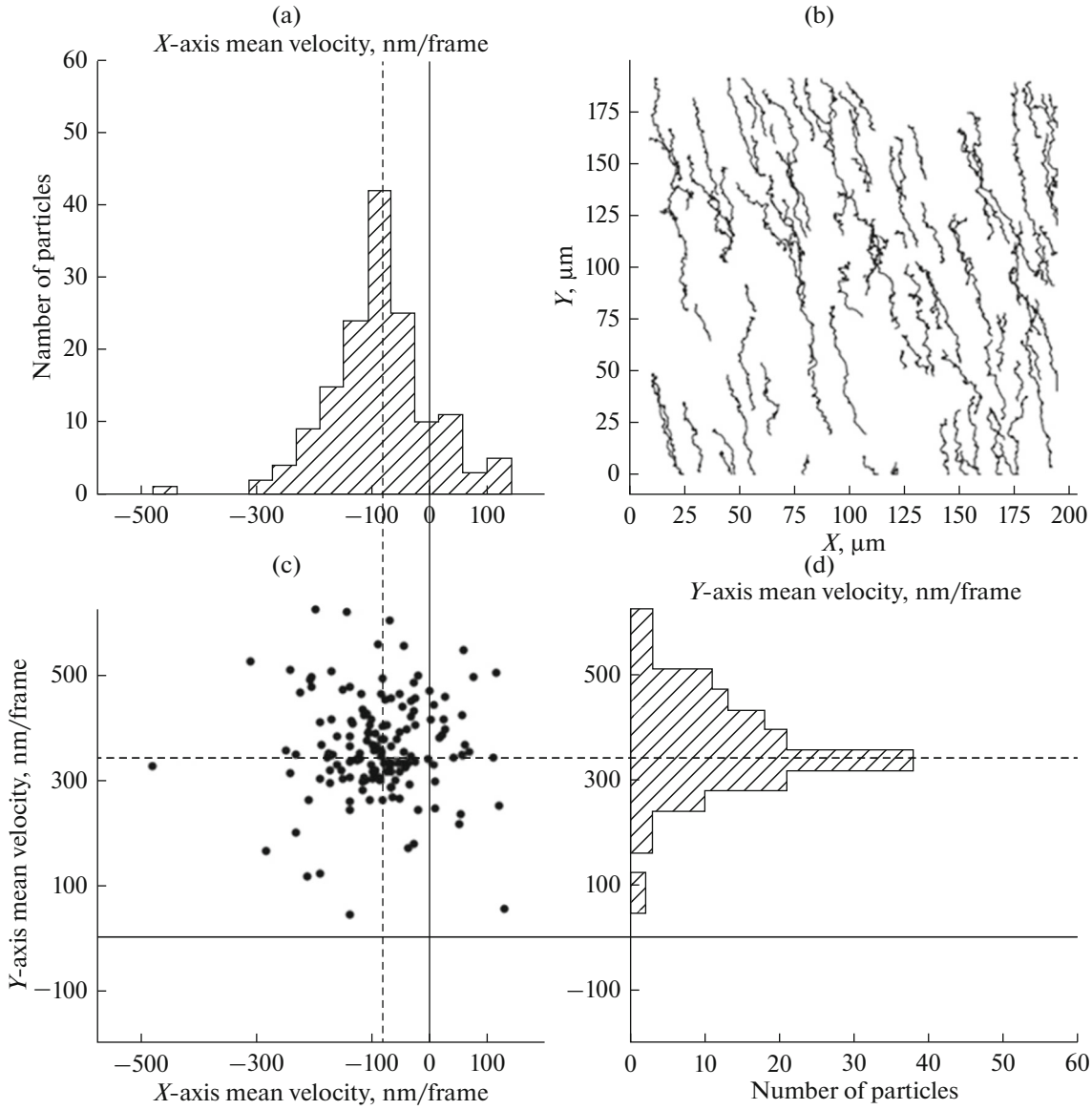

Fig. 3. Example of recording trajectories of Brownian motion of Nd^{3+}:LaF_3 nanoparticles in water in the presence of convection: (b) trajectories obtained by analyzing recorded images, histograms of mean velocities of recorded nanoparticles in the (a) vertical and (d) horizontal directions, and (c) the calculated mean velocities of nanoparticles in the vertical and horizontal directions.

nient to use R_h, because it can be measured experimentally, for example, by the NTA method, which makes it possible to determine the individual R_h value, and by the DLS method, which makes it possible to determine the ensemble-averaged R_h value for nanoparticles in solution. Additional information on the cluster spatial structure can be derived from the ratio $\rho = R_g/R_h$, which is often used to analyze the morphology of branched structures, e.g., branched macromolecules [19]. Its value for close-packed structures is less than unity and tends to $\rho \approx 0.8$ for a homogeneous sphere. However, in the case of nontrivial mass distribution, this ratio may exceed unity; for example, $\rho \approx 1.7$, as occurs for coils of linear macromolecules [20] or fractal-like aggregates [21].

In terms of the concept widely accepted in the literature, clusters of colloidal nanoparticles are well described by the fractal model (see, e.g., [22–24]). Within this model, the fractal dimension D_f is used to describe the complex spatial distribution of a cluster consisting of identical particles. This parameter is found from the expression

$$N = k_f \left(\frac{R_g}{r} \right)^{D_f}, \quad (3)$$

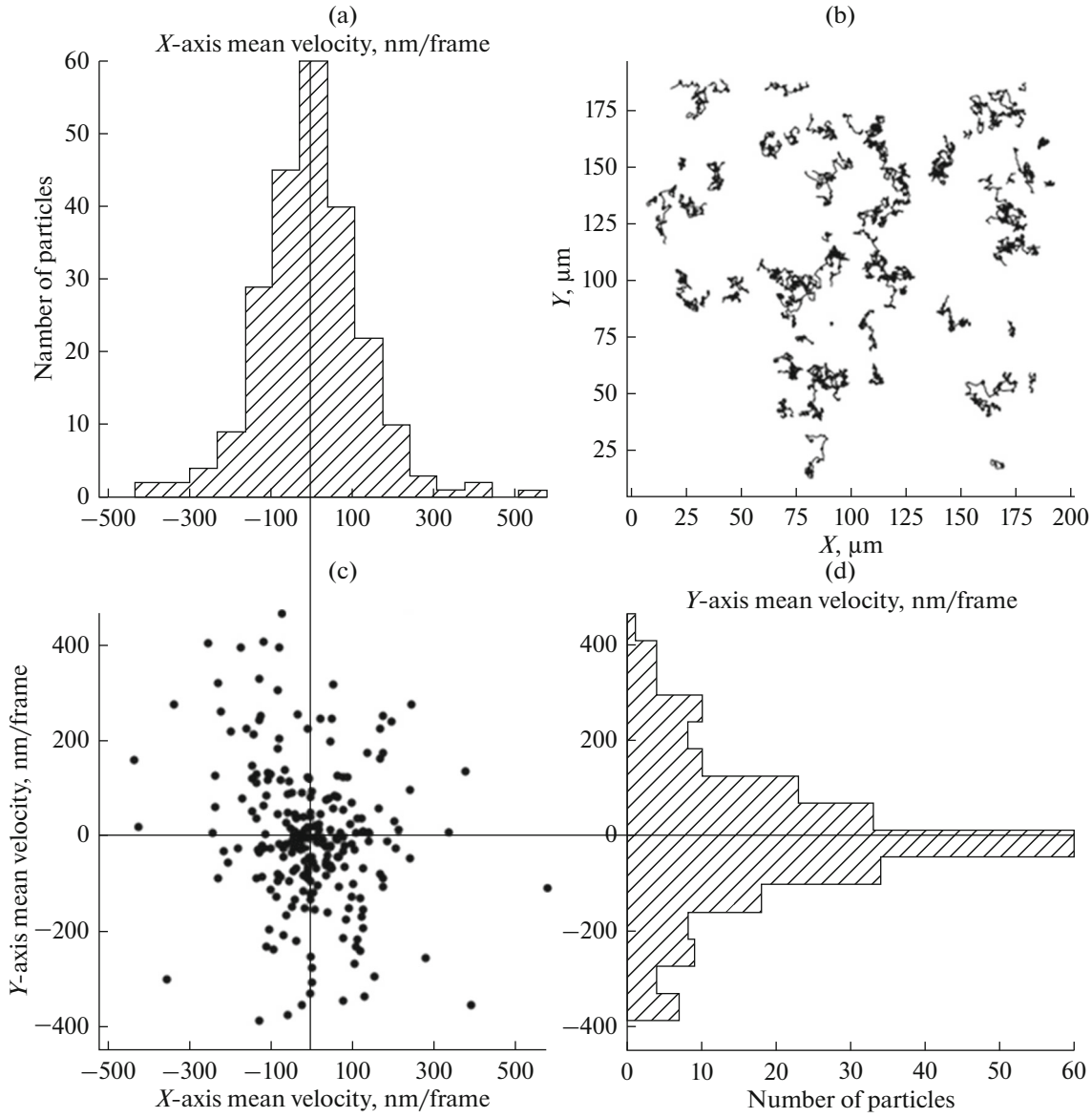

Fig. 4. Example of detection and analysis of the trajectories of Brownian motion of detected Nd^{3+}:LaF_3 nanoparticles in water in the absence of convection: (b) trajectories obtained by analyzing recorded images; the distribution histograms of nanoparticle velocities in the (a) vertical and (d) horizontal directions are almost symmetric with respect to the zero velocity. The centroid of the two-dimensional distribution of calculated nanoparticle velocities (c) almost coincides with the zero velocity.

which relates the number of primary particles constituting a cluster N, with the cluster radius of gyration [22] in the form of a power law. Here, r is the radius of primary particles and k_f is a factor, which ranges from 1 to 1.2 and depends on D_f [25]:

$$k_f = 4.46D_f^{-2.08}. \quad (4)$$

Clusters with a dimension D_f close to 3 are close-packed structures with a close-to-uniform mass distribution. Clusters with D_f close to unity have a shape similar to "filamentary" [26]. At $1.75 < D_f < 2.1$ clusters demonstrate a "loose" (in particular, fractal) structure. In most studies devoted to colloidal nanoparticles the structure of the clusters formed by these particles in solutions is described as fractal, with a dimension D_f ranging from 1.75 to 2.1.

The TEM images recorded in our experiments demonstrate a small number of single nanoparticles and a much larger number of clusters based on them; these clusters consist of densely packed cores and branches. This structure has little in common with a fractal one, which is characterized by a loose, relatively uniform distribution of the particles forming the cluster. The presence of separate branches should lead to an increase in the hydrodynamic resistance of these clusters, and the close packing of nuclei should

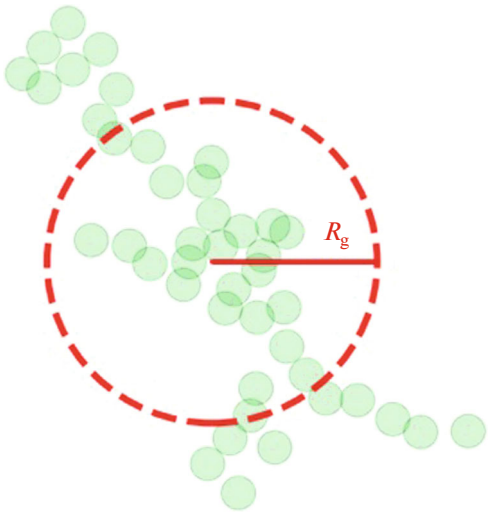

Fig. 5. (Color online) Relationship between the radius of gyration and a set of constituting particles on the example of a model cluster consisting of identical particles.

decrease the cluster radius of gyration. This suggestion is confirmed by our measurement results.

Figure 7 shows distributions of the effective sizes of primary nanoparticles and clusters based on them, calculated from the obtained TEM images: (a) distribution of the radii of spheres of equivalent-area (black line) for primary nanoparticles; (b) distribution of the R_g values for the clusters (red line); and (c) distribution of the R_h values measured for nanoparticles in water using the NTA (green line) and DLS (blue line) methods. The distribution of the equivalent radii of primary nanoparticles is fairly narrow, with a maximum near 9 nm and a width of ~12 nm. The other distributions are characterized by much larger values of maxima and widths.

The distributions of R_h values for Nd^{3+}:LaF_3 nanoparticles (see Fig. 7) show that their maxima found by the NTA and DLS methods (47 and 45 nm, respectively) coincide with good accuracy, which indicates objectivity of the data obtained by two different methods. At the same time, the shapes of these distributions significantly differ, which can be explained by the fundamental difference between these methods. NTA provides information about the hydrodynamic radius of each nanoparticle taken separately, giving idea about the real shape of the distribution of radii, whereas the DLS method, being integral, yields only averaged information about the shape of R_h distribution. In particular, when processing the data obtained by this method, the distribution shape is set by fitting an approximating function and is not the measurement result (in our case, a Gaussian function was chosen for approximation). At the same time, the distribution of the R_g values for nanoparticles, obtained by processing TEM images, is asymmetric, similar to the distribution obtained by NTA, which can be described by the sum of two Gaussians. This coincidence may suggest objectivity of the obtained result, indicating the presence of two types of clusters with different parameters in a solution. Presumably, these may be

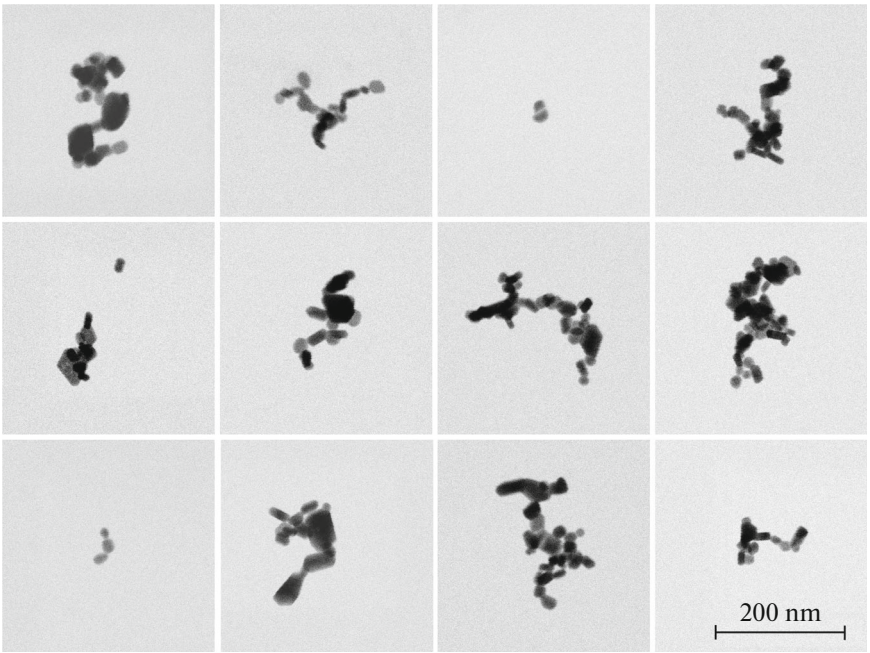

Fig. 6. Examples of TEM images of nanoclusters formed on the basis of colloidal Nd^{3+}:LaF_3 nanoparticles, spin-coated on a rapidly rotating carbon substrate.

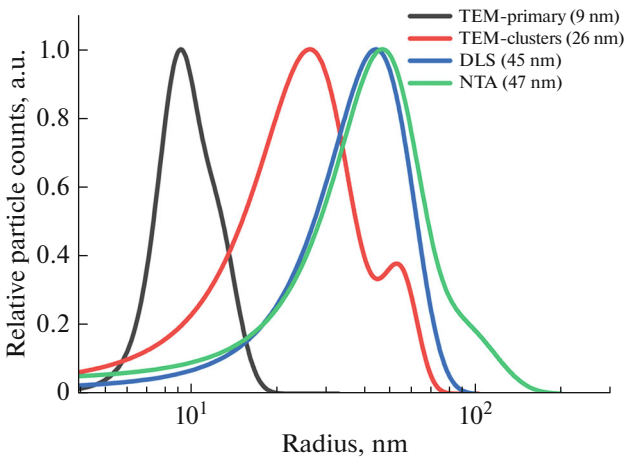

Fig. 7. (Color online) Distributions of sizes of primary colloidal Nd^{3+}:LaF_3 nanoparticles and effective sizes of the clusters formed on their basis: (black line) distribution of the radii of equivalent spheres for primary nanoparticles; (red line) distribution of the radii of gyration of clusters; and (green and blue lines) distributions of the hydrodynamic radius of clusters, found by the NTA and DLS methods, respectively. The black line is the result of numerical analysis of individual sizes of nanoparticles (radii of spheres with equivalent areas), disregarding their aggregation; the red line characterizes the effective sizes of clusters, calculated as their radii of gyration; and the green and blue lines are values of hydrodynamic radii of clusters, determined using the ultramicroscope and DLS method, respectively.

(i) aggregates formed directly during synthesis and (ii) larger aggregates, formed in later stages (including the solution storage).

Let us analyze the ratio of the R_g and R_h values, $\rho = R_g/R_h$, for the clusters measured in this study. As can be seen in Fig. 7, the distribution of R_g values is noticeably shifted to smaller ones in comparison with the R_h values. The ratio of the maxima of the corresponding distributions is 0.7, which is smaller than the corresponding value for fractal-like clusters ($\rho \approx 1.75$) [21]. This discrepancy may be caused by the difference in their morphology. In the case of fractal-like clusters, which are loose structures distributed in space (Fig. 8a), many primary particles are located far from the center, which leads to an increase in the R_g value in comparison with R_h. For closely packed primary particles (Fig. 8b), ρ approaches the value of 0.8, which characterizes a homogeneous sphere. For a cluster consisting of a dense core with a small R_g value and small number of branches that increase the hydrodynamic resistance of the cluster (Fig. 8c), the R_h value can significantly increase and, accordingly, ρ can decrease.

The above simplified consideration provides a possible explanation of the difference of the ρ value found in our experiments from the value predicted by the fractal model and suggests that the spatial structure of the clusters studied here corresponds to a greater extent to the clusters consisting of a relatively small dense core and several branches.

4. TEMPORAL STABILITY OF COLLOIDAL SOLUTION

Processes of aggregation of nanoparticles are closely related to their chemical properties and the impacts of these nanoparticles on biological objects. Examples are different velocities of migration of aggregates and single nanoparticles in biological media; possibility of activation of the phagocytosis mechanisms in cells; and other effects, related to the cluster sizes and structure [27], especially in biology and medicine. In this study, we investigated the temporal stability of synthesized nanoparticles and their resistance to aggregation. As mentioned above, the values of their ζ potential (a parameter widely used to estimate the resistance of a colloidal solution to aggregation) were measured. Our measurements of the ζ potential gave a fairly large value ($47 \pm 5\%$ mV), which suggests that the solution of synthesized nanoparticles has a high temporal stability.

To verify this, we performed control measurements of the shape of distribution of hydrodynamic radii of synthesized nanoparticles in a relatively fresh solution (kept for three days after preparation) and in a solution stored for a long time (seven months). The results of these measurements are shown in Fig. 9.

Measurements were performed with a solution that was not subjected to treatment in an ultrasonic bath, as well as with a solution that underwent this treatment. The obtained distributions demonstrate that the distribution maximum for the colloidal solution of nanoparticles stored for a long time shifts to larger sizes, which may suggest occurrence of larger aggregates due to the aggregation of initial clusters. It is noteworthy that the observed aggregation effect was partially eliminated after exposure of the sample to ultrasound. One can suggest that bonds of two types arise between primary nanoparticles during aggregation: a weak bond (apparently, of the van-der-Waals type) and a stronger one (apparently, electrostatic). Thus, the results obtained demonstrate a high temporal stability of synthesized colloidal solution, as well as the presence of a contribution from irreversible processes of nanoparticle aggregation.

It should also be noted that the obtained data on the processes of nanoparticle aggregation in solutions of the synthesized nanoparticles are preliminary and insufficient for a complete understanding of their nature and the development of effective methods for their weakening. Therefore, the research in this field should be continued to get greater clarity on these important issues.

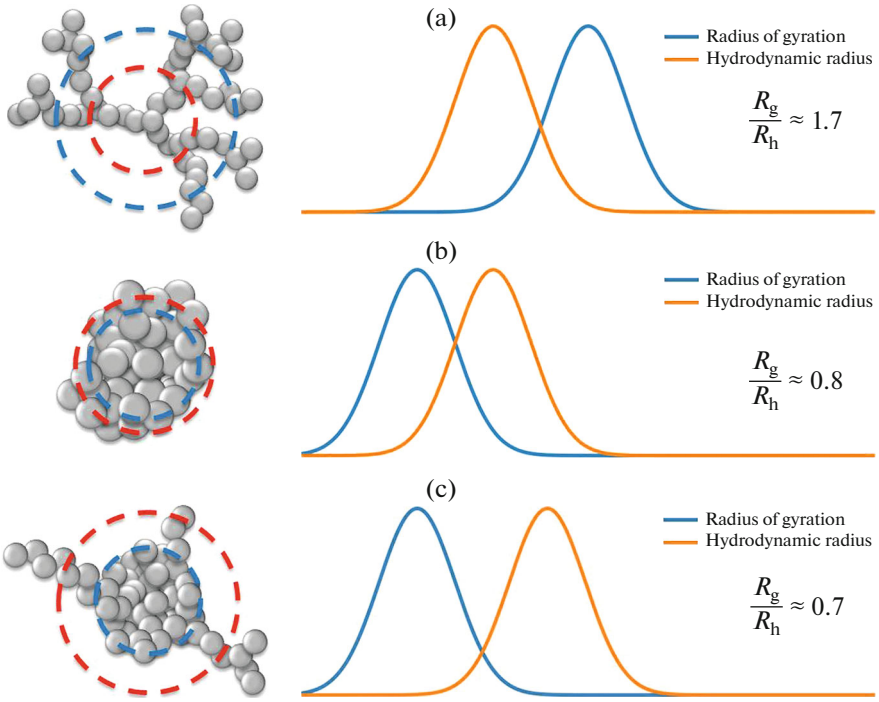

Fig. 8. (Color online) Hypothetical distributions of the hydrodynamic radius and radius of gyration for different nanoclusters. (a) Nanocluster with a fractal structure, for which the mass distribution is such that most of the mass is located far from the center of mass; due to this, the radius of gyration significantly increases and may exceed the hydrodynamic radius. (b) Close-packed cluster, for which the distributions of R_g and R_h are close to those for a homogeneous sphere. (c) Nanocluster in the form of a dense core with few branches, which increase the hydrodynamic radius to a greater extent than the radius of gyration, as a result of which the ρ value for this cluster becomes smaller than for a homogeneous sphere.

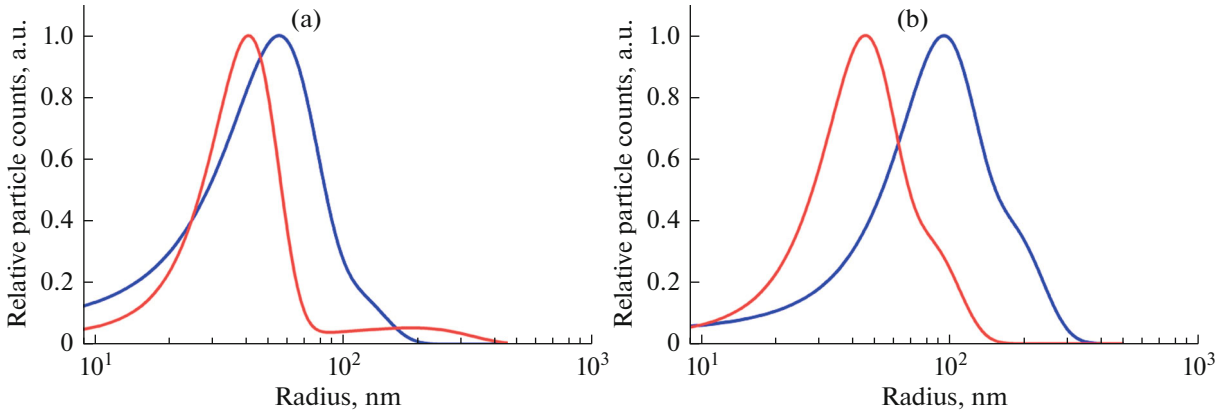

Fig. 9. (Color online) Size distributions of colloidal Nd^{3+}:LaF_3 nanoparticles, measured with the ultramicroscope (a) three days after the sample preparation and (b) after seven-month storage: results obtained (red lines) after ultrasonic treatment of the colloidal solution and (blue lines) without any preliminary preparation.

5. CONCLUSIONS

The size distribution and spatial structure of colloidal lanthanum fluoride nanoparticles doped with Nd^{3+} ions, synthesized in an aqueous solution by the hydrothermal method with subsequent microwave treatment, and nanoclusters formed on their basis were studied using highly sensitive optical ultramicroscopy of elastic scattering and transmission electron microscopy. A comparative analysis of the size distributions obtained by two different methods showed that the mean hydrodynamic radius of nanoclusters exceeds their mean radius of gyration. This result contradicts the predictions of the fractal model, which is widely used to describe the spatial structure of colloidal nanoclusters: according to this theory, the

hydrodynamic radius of clusters should be smaller than their radius of gyration.

An analysis of the TEM images of nanoclusters studied shows that their spatial structure is better described by a combination of a close-packed cores with several thread-like branches, whereas fractal-like clusters are described by a "loose" structure.

Thus, the results obtained by two different experimental methods give grounds to draw an important conclusion: the fractal model of colloidal nanoparticles is not suitable to describe the spatial structure of synthesized nanoclusters.

The results of multi-month studies of the temporal stability of aqueous solutions of synthesized colloidal nanoparticles showed that they extremely slowly aggregate during long-term storage at room temperature. It was shown that, under the action of ultrasound, the observed aggregation can be reverted to a great extent, which indicates weakness of the newly formed bonds. An analysis of high-resolution TEM images of nanoclusters did not reveal the joint growth of primary nanoparticles during storage.

FUNDING

Synthesis of lanthanum fluoride nanoparticles and the studies using laser dark-field microscopy and electron transmission microscopy were supported by the Russian Science Foundation, grant no. 22-22-00998. The development of the method for synthesizing lanthanum fluoride nanoparticles was supported by the Estonian Research Council, grant no. PRG347.

CONFLICT OF INTEREST

The authors declare that they have no conflicts of interest.

REFERENCES

1. A. Popov, E. Orlovskaya, A. Shaidulin, E. Vagapova, E. Timofeeva, L. Dolgov, L. Iskhakova, O. Uvarov, G. Novikov, M. Rähn, A. Tamm, A. Vanetsev, S. Fedorenko, S. Eliseeva, S. Petoud, and Y. Orlovskii, "Stable aqueous colloidal solutions of Nd^{3+}:LaF_3 nanoparticles, promising for luminescent bioimaging in the near-infrared spectral range," *Nanomaterials* **11** (11), 2847 (2021). https://doi.org/10.3390/nano11112847
2. Y. Orlovskii, A. Popov, E. Orlovskaya, A. Vanetsev, E. Vagapova, M. Rähn, V. Sammelselg, I. Sildos, A. Baranchikov, P. Grachev, V. Loschenov, and A. Ryabova, "Comparison of concentration dependence of relative fluorescence quantum yield and brightness in first biological window of wavelengths for aqueous colloidal solutions of Nd^{3+}:LaF_3 and Nd^{3+}:KY_3F_{10} nanocrystals synthesized by microwave-hydrothermal treatment," *J. Alloys Compd.* **756**, 182–192 (2018). https://doi.org/10.1016/j.jallcom.2018.05.027
3. Y. Yang, J. Aw, and B. Xing, "Nanostructures for NIR light-controlled therapies," *Nanoscale* **9** (11), 3698–3718 (2017). https://doi.org/10.1039/C6NR09177F
4. B. del Rosal, A. Pérez-Delgado, M. Misiak, A. Bednarkiewicz, A. S. Vanetsev, Yu. Orlovskii, D. J. Jovanović, M. D. Dramićanin, U. Rocha, K. U. Kumar, C. Jacinto, E. Navarro, E. M. Rodríguez, M. Pedroni, A. Speghini, G. A. Hirata, I. R. Martín, and D. Jaque, "Neodymium-doped nanoparticles for infrared fluorescence bioimaging: The role of the host," *J. Appl. Phys.* **118** (14), 143104 (2015). https://doi.org/10.1063/1.4932669
5. D. H. Ortgies, F. J. Teran, U. Rocha, L. de la Cueva, G. Salas, D. Cabrera, A. S. Vanetsev, M. Rähn, V. Sammelselg, Yu. V. Orlovskii, and D. Jaque, "Optomagnetic nanoplatforms for in situ controlled hyperthermia," *Adv. Funct. Mater.* **28** (11), 1704434 (2018). https://doi.org/10.1002/adfm.201704434
6. U. Rocha, J. Hu, E. M. Rodríguez, A. S. Vanetsev, M. Rähn, V. Sammelselg, Yu. V. Orlovskii, J. G. Solé, D. Jaque, and D. H. Ortgies, "Subtissue imaging and thermal monitoring of gold nanorods through joined encapsulation with Nd-doped infrared-emitting nanoparticles," *Small* **12** (39), 5394–5400 (2016). https://doi.org/10.1002/smll.201600866
7. P. Hole, "Particle tracking analysis (PTA)," in *Characterization of Nanoparticles: Measurement Processes for Nanoparticles*, Ed. by V.-D. Hodoroaba, W. E. S. Unger, and A. G. Shard (Elsevier, Amsterdam, 2020), Chap. 3.1.2, pp. 79–96. https://doi.org/10.1016/b978-0-12-814182-3.00007-9
8. J. Stetefeld, S. A. McKenna, and T. R. Patel, "Dynamic light scattering: A practical guide and applications in biomedical sciences," *Biophys. Rev.* **8**, 409–427 (2016). https://doi.org/10.1007/s12551-016-0218-6
9. V. Filipe, A. Hawe, and W. Jiskoot, "Critical evaluation of nanoparticle tracking analysis (NTA) by NanoSight for the measurement of nanoparticles and protein aggregates," *Pharm. Res.* **27** (5), 796–810 (2010). https://doi.org/10.1007/s11095-010-0073-2
10. E. Timofeeva, E. Orlovskaya, A. Popov, A. Shaidulin, S. Kuznetsov, A. Alexandrov, O. Uvarov, Y. Vainer, G. Silaev, M. Rähn, A. Tamm, S. Fedorenko, and Y. Orlovskii, "The influence of medium on fluorescence quenching of colloidal solutions of the Nd^{3+}:LaF_3 nanoparticles prepared with HTMW treatment," *Nanomaterials* **12** (21), 3749 (2022). https://doi.org/10.3390/nano12213749
11. L. Scriven, "Physics and applications of DIP coating and spin coating," *MRS Proc.* **121**, 717–729 (1988). https://doi.org/10.1557/PROC-121-717
12. J. Goodman, "Some fundamental properties of speckle," *J. Opt. Soc. Am.* **66** (11), 1145–1150 (1976). https://doi.org/10.1364/JOSA.66.001145
13. C. A. Schneider, W. S. Rasband, and K. W. Eliceiri, "NIH Image to ImageJ: 25 years of image analysis," *Nat. Methods* **9**, 671–675 (2012). https://doi.org/10.1038/nmeth.2089
14. J.-Y. Tinevez, N. Perry, J. Schindelin, G. M. Hoopes, G. D. Reynolds, E. Laplantine, S. Y. Bednarek, S. L. Shorte, and K. W. Eliceiri, "TrackMate: An open and extensible platform for single-particle tracking,"

Methods **115**, 80–90 (2017).
https://doi.org/10.1016/j.ymeth.2016.09.016

15. C. L. Vestergaard, P. C. Blainey, and H. Flyvbjerg, "Optimal estimation of diffusion coefficients from single-particle trajectories," *Phys. Rev. E* **89** (2), 022726 (2014).
https://doi.org/10.1103/PhysRevE.89.022726
16. T. Wagner, H.-G. Lipinski, and M. Wiemann, "Dark field nanoparticle tracking analysis for size characterization of plasmonic and non-plasmonic particles," *J. Nanopart. Res.* **16** (5), 2419 (2014).
https://doi.org/10.1007/s11051-014-2419-x
17. M. Altenhoff, S. Aßmann, C. Teige, F. J. Huber, and S. Will, "An optimized evaluation strategy for a comprehensive morphological soot nanoparticle aggregate characterization by electron microscopy," *J. Aerosol Sci.* **139**, 105470 (2020).
https://doi.org/10.1016/j.jaerosci.2019.105470
18. Ü. Ö. Köylü, G. M. Faeth, T. L. Farias, and M. G. Carvalho, "Fractal and projected structure properties of soot aggregates," *Combust. Flame* **100** (4), 621–633 (1995).
https://doi.org/10.1016/0010-2180(94)00147-K
19. W. Burchard, "Solution properties of branched macromolecules," in *Branched Polymers II: Advances in Polymer Science*, Ed. by J. Roovers (Springer, Berlin–Heidelberg, 1999), Vol. 143, pp. 113–194.
https://doi.org/10.1007/3-540-49780-3_3
20. S. Kadlubowski, "Radiation-induced synthesis of nanogels based on poly(N-vinyl-2-pyrrolidone)—A review," *Radiat. Phys. Chem.* **102**, 29–39 (2014).
https://doi.org/10.1016/j.radphyschem.2014.04.016
21. M. Lattuada, H. Wu, and M. Morbidelli, "Hydrodynamic radius of fractal clusters," *J. Colloid Interface Sci.* **268** (1), 96–105 (2003).
https://doi.org/10.1016/j.jcis.2003.07.028
22. A. M. Brasil, T. L. Farias, and M. G. Carvalho, "A recipe for image characterization of fractal-like aggregates," *J. Aerosol Sci.* **30** (10), 1379–1389 (1999).
https://doi.org/10.1016/S0021-8502(99)00026-9
23. C. M. Sorensen, "Light scattering by fractal aggregates: A review," *Aerosol Sci. Technol.* **35** (2), 648–687 (2001).
https://doi.org/10.1080/02786820117868
24. H. Wu, M. Lattuada, and M. Morbidelli, "Dependence of fractal dimension of DLCA clusters on size of primary particles," *Adv. Colloid Interface Sci.* **195–196**, 41–49 (2013).
https://doi.org/10.1016/j.cis.2013.04.001
25. L. Ehrl, M. Soos, and M. Lattuada, "Generation and geometrical analysis of dense clusters with variable fractal dimension," *J. Phys. Chem. B* **113** (31), 10587–10599 (2009).
https://doi.org/10.1021/jp903557m
26. S. Lazzari, L. Nicoud, B. Jaquet, M. Lattuada, and M. Morbidelli, "Fractal-like structures in colloid science," *Adv. Colloid Interface Sci.* **235**, 1–13 (2016).
https://doi.org/10.1016/j.cis.2016.05.002
27. E. Hotze, T. Phenrat, and G. Lowry, "Nanoparticle aggregation: Challenges to understanding transport and reactivity in the environment," *J. Environ. Qual.* **39** (6), 1909–1924 (2010).
https://doi.org/10.2134/jeq2009.0462

Translated by Yu. Sin'kov